Materials Science & Engineering A 759 (2019) 203–209

Contents lists available at ScienceDirect

Materials Science & Engineering A

journal homepage: www.elsevier.com/locate/msea

Dynamic compression-induced twins and martensite and their combined effects on the adiabatic shear behavior in a Ti-8.5Cr-1.5Sn alloy

Huiliang Yang[a,b], Duoduo Wang[a,b], Xinjie Zhu[a,b], Qunbo Fan[a,b,*]

[a] School of Materials Science and Engineering, Beijing Institute of Technology, Beijing, 100081, China
[b] National Key Laboratory of Science and Technology on Materials under Shock and Impact, Beijing Institute of Technology, Beijing, 100081, China

ARTICLE INFO

Keywords:
Twins
Martensite
Adiabatic shear band
Plastic deformation degree
Titanium

ABSTRACT

The samples cut from the Ti-8.5Cr-1.5Sn titanium alloy were prepared to explore the combined effects of dynamic compression-induce twins and martensite on the adiabatic shear behavior. The morphologies of the deformed microstructures were examined by means of optical microscopy (OM), scanning electron microscopy (SEM), and transmission electron microscopy (TEM) observations, which revealed a high density of twins and martensite. The volume fraction of these features increased when the strain rate increased from 1000/s to 1500/s, owing to the relatively large driving force associated with twinning induced plasticity (TWIP) and transformation induced plasticity (TRIP) effects. Such phenomena resulted in an increase in the unit strain increment (induced by the unit stress increment $\Delta\varepsilon$ / $\Delta\sigma$) and the energy absorbed. At strain rates of 2000/s or higher, adiabatic shear failure occurred and the values of $\Delta\varepsilon$ / $\Delta\sigma$ and the absorbed energy were far greater than that at 1500/s. The twins and martensite around the adiabatic shear bands (ASBs) were broken due to severe local deformation and subsequent dynamic recrystallization. Furthermore, the presence of twins and martensite induced (in general) bifurcation of the ASBs, which played a crucial role in the plasticity of the alloy.

1. Introduction

Titanium and its alloys are increasingly used for aerospace, biomedical, and automotive applications due to their low density, good corrosion resistance, and high strength-to-density ratio [1–3]. However, these alloys are particularly susceptible to adiabatic shear localization during dynamic loading, owing to their low thermal conductivity. Adiabatic shear localization is an important failure mechanism, which often occurs during the high-strain-rate deformation of materials [4–7]. This mechanism is generally characterized as a plastic flow instability phenomenon, where thermal softening arising from the adiabatic temperature rise exceeds work hardening and strain-rate hardening [8,9]. In recent years, adiabatic shear bands (ASBs) in titanium alloys have received considerable attention, and numerous studies, including those focused on microstructural evolution and theoretically based explanations, have been conducted on adiabatic shear localization in titanium and its alloys. The results revealed that many twins are generated around the ASBs after dynamic loading of some titanium alloys [10–12]. Furthermore, in some cases, martensite forms in alloys such as Ti–6Al–4V [12], Ti-5553 alloy [13], and β-CEZ Ti alloy [14].

Twinning, as an important form of plastic deformation, contributes directly to crystal deformation, and leads to changes in crystal orientation. Similarly, the deformation twins generated during the deformation process of the alloy reduce the effective distance of the dislocation slip, resulting in improved strength and plasticity of the alloy via the twinning induced plasticity (TWIP). Marquis et al. [15] and Venkatesh et al. [16] found that twins in titanium alloys increase the quasi-static mechanical properties of the material. Moreover, Osovski [17] performed a systematic comparison of pure titanium and Ti6Al4V, and found that twinning will lead to significant delays in the occurrence of dynamic recrystallization (DRX). This results in pure titanium with superior resistance to adiabatic shear failure. Osovski proposed that twins are an active source of dissipation, which therefore delays DRX occurrence and consequently shear localization. Sun et al. [18] performed high-speed compression tests on metals with different structures. The results showed that different twin boundary orientations have non-equivalent effects on ASBs. For example, twins parallel to the shear direction were gradually broken, while those perpendicular to the shear direction hindered the expansion of the shear band.

Martensitic transformation can also be used to improve the properties of the material. Zackey et al. [19] investigated the mechanical properties of high-strength steels. The results revealed that martensitic transformation can maintain good plasticity while strengthening the material during deformation. Therefore, the concept of a

* Corresponding author. School of Materials Science and Engineering, Beijing Institute of Technology, Beijing, 100081, China.
E-mail address: fanqunbo@bit.edu.cn (Q. Fan).

https://doi.org/10.1016/j.msea.2019.05.040
Received 4 March 2019; Received in revised form 30 April 2019; Accepted 11 May 2019
Available online 13 May 2019

transformation induced plasticity (TRIP) effect was proposed. Since then, the TRIP effect has been extensively investigated, and its application to titanium alloy has been widely promoted. Brozek et al. [20] systematically studied the stress-induced martensitic transformation in Ti–Cr based alloys and found that the TRIP effect can improve the mechanical properties of the alloy. Furthermore, Yan et al. [21] designed a near-α titanium alloy with the TRIP effect, which improved the strength and plasticity of the alloy. Unfortunately, most studies have focused on quasi-static conditions, and only a few have considered high-strain-rate deformation. Xu et al. [13] investigated the dynamic properties of a Ti-5553 alloy via Split Hopkinson Pressure Bar and light gas gun experiments. The results revealed that a martensitic transformation zone occurs around the ASBs, and the grains in this area were severely elongated. Eskandari et al. [22] systematically investigated the formation of ASB and plastic deformation mechanisms within neighboring grains by high-resolution electron backscatter diffraction in Mn-steel, and some significant results were obtained. It was found that formation of athermal ε-martensite and ά-martensite within the shear bands induced a brittle intersection structure and resulted in crack initiation and propagation in this region. Moreover, the formation of twins towards the ASB suggested that mechanical twinning occurred in the neighbor grains.

However, studies focusing on the influence of both twins and martensite on the adiabatic shear behavior of the alloy are rare, although this behavior is critical to improving the performance of materials under dynamic loading. In this work, we studied a new β-type titanium alloy, Ti-8.5Cr-1.5Sn, which was designed by Brozek et al. [23] in accordance with the "d-electron alloy theory" [24–26] proposed by Morinaga. Twins and martensite can occur simultaneously in this alloy, if the material is subjected to certain heat treatment and deformation conditions. The effect of these features on the adiabatic shear behavior will be discussed in the current study.

2. Experimental

The Ti-8.5Cr-1.5Sn titanium alloy (see Table 1 for the chemical composition) was smelted in a 10-kg vacuum induction furnace. A 40 mm × 40 mm × 13 mm block sample was cut out from the ingot (see Fig. 1(a)). Subsequently, the sample was preheated for 20 min at 1073 K, and then rolled to 7 mm (via 10 paths) in the thickness direction, as shown in Fig. 1(b). A final cumulative reduction of 46% was realized. After the rolling, the hot-rolled plate was air-cooled to room temperature, annealed at 1173 K for 120 min, and then water cooled. Afterward, 5 mm (diameter) × 5 mm (height) samples (see Fig. 1(c)) were cut from the plate. These samples were then subjected to dynamic loading tests using a Split Hopkinson Pressure Bar at room temperature. Through wire-electrode cutting, samples for microstructural characterization were cut from the dynamically deformed samples along the loading axis.

Metallographic specimens were prepared via standard mechanical polishing and subsequent etching in a solution of 2 mL hydrofluoric acid + 18 mL nitric acid + 80 mL distilled water. The microstructural characteristics were examined with a OlympusPME-3 optical microscope. Moreover, the microstructural features of the titanium alloy after dynamic loading were examined via scanning electron microscopy conducted on a Quanta 200F field-emission scanning electron microscope at 15 kV.

Samples for TEM were cut out to a 500-μm foil along the loading axis, and then mechanically ground to a thickness of 30–50 μm. A 3-mm-diameter disk was carefully punched out from the foil to ensure that the shear band paths cross the center of the disk. Afterward, electrolytic polishing was conducted for 90 s at 40 V and -30 K on a twin-jet polisher using a solution of 60 mL perchloric acid + 360 mL n-butyl alcohol + 600 mL methanol. TEM observation was performed on a Tecnai F30 transmission electron microscope operated at 300 kV.

Table 1
Chemical composition of the titanium alloy (wt.%).

Material	Cr	Sn	Fe	Si	Ti
Ti-8.5Cr-1.5Sn	8.5	1.5	0.02	0.02	Balance

3. Results and discussion

3.1. The appearance of twins and martensite

Fig. 2(a) shows an optical micrograph of the alloy after heat treatment. After this treatment, the alloy undergoes dynamic compression loading (see resulting microstructure in Fig. 2(b)). The initial heat treated sample has equiaxed β grains with diameter ranging from 200 to 300 μm, as shown in Fig. 2(a). No twin-like and martensite-like structures were found in the grains. The heated alloy is composed of equiaxed grains. However, many twin-like and martensite-like structures are generated during dynamic loading. These structures were elucidated via TEM investigation. Fig. 3 shows TEM images of the alloy after heat treatment and subsequent dynamic compression. Fig. 3(a) shows the lath-like structure present in the β grain, and the corresponding selected area electron diffraction pattern reveals that the structure is martensite. The strain-induced martensite (width: 150 nm–200 nm) is arranged parallel to the longitudinal axis of the alloy. In addition, very tiny secondary martensite (width: 60 nm) is also observed (see dashed rectangle in Fig. 3(a)). The lath-like structure is accompanied by other parallel structures in the alloy (as shown in Fig. 3(b)), which can be identified as twins from a conventional selected area diffraction pattern. This indicates that TRIP and TWIP effects can occur simultaneously.

3.2. The effect of strain rate on twins and martensite

Since the samples were tested by a Split Hopkinson Pressure Bar, the stress, strain and strain rate can be calculated from the data collected by the strain gauge recordings on the incident bar and transmitter bar. The strain rate responses for the alloy are plotted as a function of time in Fig. 4. It is clear from Fig. 4 that the strain rates measured from the SHPB test are not constant. Generally, the value at relative stable plateau can be regarded as an average strain rate [27,28]. So, the average strain rate of curve 1, 2, and 3 are 1000/s, 1500/s, and 2000/s, respectively.

As mentioned in Section 3.1, there is no twins and martensite generated in the annealed alloy (see Fig. 2(a)), but a large number of twins and martensite can be found from the optical micrograph of the alloy at strain rate of 1000/s, 1500/s, and 2000/s shown in Fig. 5. As Fig. 5 (a) and (b) show, the alloy can be roughly divided into two areas: less volume fraction of twins and martensite (denoted as Area **I**), more volume fraction of twins and martensite (denoted as Area **II**). It can be clearly seen that, at strain rate of 1500/s, there are more Area II present in the alloy compared to the alloy at strain rate of 1000/s, where the arrangement of twins and martensite is more dense. As is well known, that twins and martensites are generated once the driving force reaches their respective critical resolved shear stresses. The different microstructure for the two strain rates indicates that generation of both TWIP and TRIP are closely related to the strain rate. To a certain degree, higher strain rate is prone to induce more twins and martensite due to a relatively larger driving force. The high volume fraction of these features occurring at a strain rate of 2000/s is accompanied by a long and narrow adiabatic shear band (width: 20 μm-50μm), which is distinct from the matrix, as shown in Fig. 5(c).

Fig. 6 shows the true stress-true strain curves of the alloy exposed to strain rates of 1000/s, 1500/s, and 2000/s. Generally, the dynamic deformation processes can be divided into three stages, namely: strain hardening stage (denoted as stage I), dynamic equilibrium stage

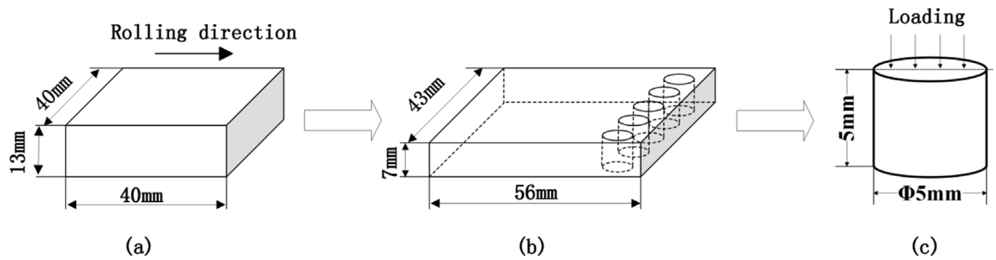

Fig. 1. Process for preparing samples: (a) before rolling; (b) after rolling; (c) the sample for dynamic compression.

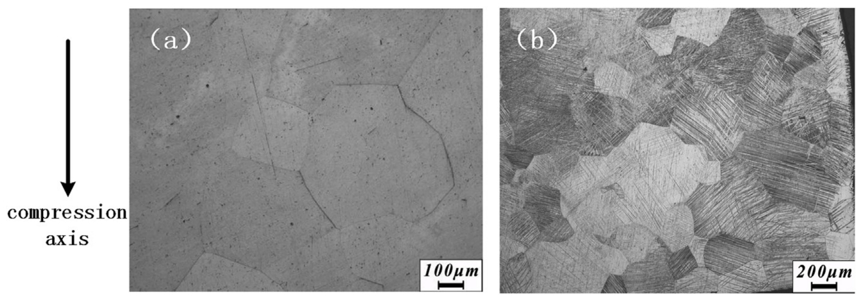

Fig. 2. Optical micrographs of the titanium alloy: (a) after heat treatment; (b) after heat treatment and subsequent dynamic compression at strain rates of 2000/s.

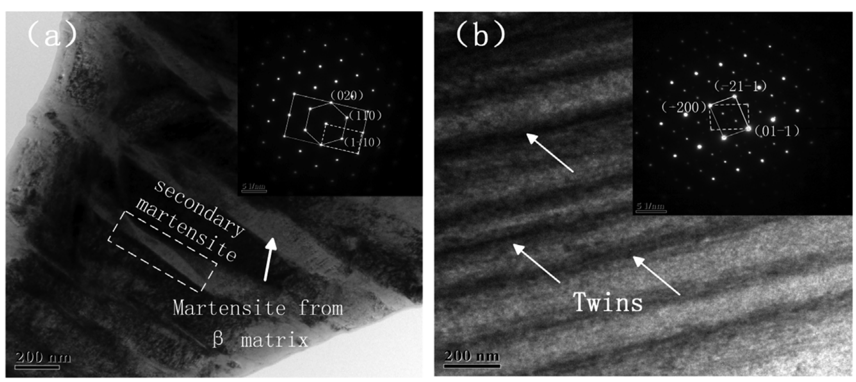

Fig. 3. TEM images of the alloy after heat treatment at 1173 K and dynamic compression at strain rates of 2000/s: TEM image and selected area diffraction pattern of (a) martensite; (b) twins.

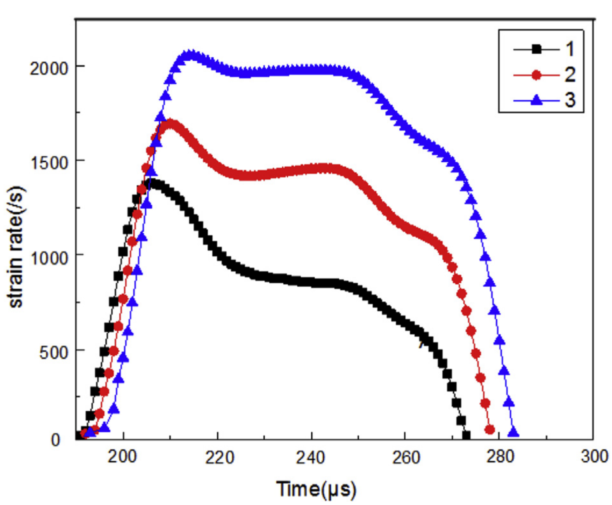

Fig. 4. Strain rate-time curve of the alloy during dynamic compression.

(denoted as stage II), and shearing instability stage (denoted as stage III). In stage I, true stress increases with the increase of true strain until achieving the peak stress. In stage II, thermal softening effect induced by the working heat is equal to hardening effect induced by the deformation, which results in a platform shown in the curves. In stage III, true stress decreases sharply with the increase of true strain which called stress collapse. The emergence of stress collapse is mainly caused by the dominant status of thermodynamic softening in the competition with work-hardening. However, owing to the lack of adiabatic shear failure at strain rates of 1000/s and 1500/s in this work, the true stress-true strain curve consists of only the first two stages. Adiabatic shear failure occurs when the strain rate of the alloy increases to 2000/s. This is manifested as an additional shearing instability stage in the curve, and the sample is broken along the direction of 45° to the compression axis.

In addition, other hardening effects and softening effects that affect the stress-strain curve shall also be noticed. As can be seen from Fig. 5, a large number of twins and martensite appear under the dynamic loading at different strain rates, which significantly contributes to work hardening capacity of the alloy. Specifically, the yield stress of the alloy, σ_y, is generally related to the grain size, d, through the Hall-Petch equation [29,30]: $\sigma_y = \sigma_0 + k_y d^{-1/2}$, where σ_0 is the friction stress and k_y is a positive constant of yielding associated with the stress required to extend dislocation activity into adjacent unyielded grains. However, the twins boundaries will lead to the increase of k_y, which increases the Hall–Petch slope [31–34]. In the process of deformation, the new

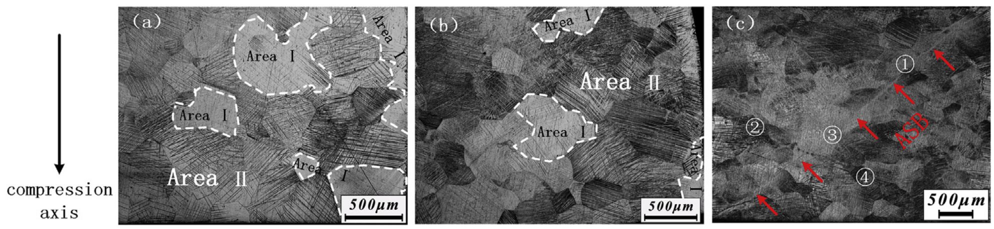

Fig. 5. Optical micrographs of the alloy at different strain rates: (a) 1000/s; (b) 1500/s; (c) 2000/s.

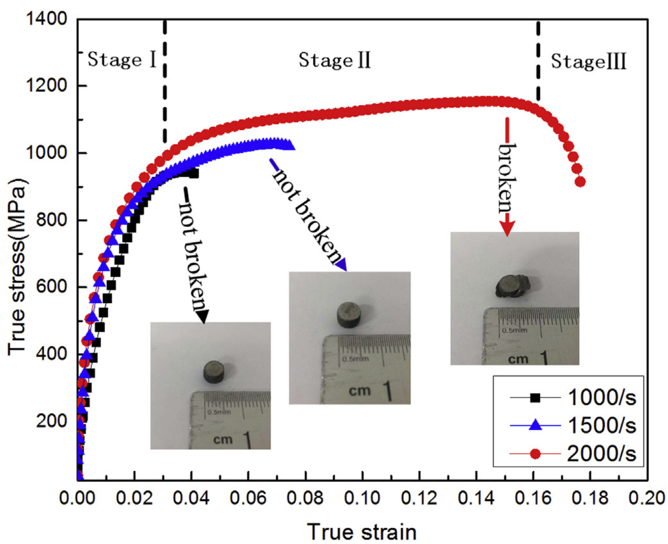

Fig. 6. Dynamic compression true stress-true strain of the alloy at different strain rates.

deformation twins and their boundaries will continue to appear, so the value of k_y will increase with the increase of the strain. At the same time, a large number of dislocations are accumulated near the newly formed twins boundaries, which hinder the dislocation motion, thus improving the strength of the alloy, and having an effect of work hardening [32,35]. Meanwhile, it has been widely reported [36–39] that the transformation of martensite has similar effect on the strengthening of the alloy in terms of the martensite plate thickness, which also conforms to Hall-Petch relationship. On the other side, however, the occurrence of DRX in the alloy would inevitably lead to the presence of a significant softening behavior in the stress-strain curve, which could bring about an important decrease in the mean flow stress [40–42].

As Fig. 6 shows, at different strain rates, the alloy experiences different unit strain increments caused by unit stress increments (hereafter defined as $\Delta\varepsilon$ / $\Delta\sigma$; see Table 2) during the dynamic equilibrium stage. At strain rates of 1000/s, 1500/s, and 2000/s, $\Delta\varepsilon$ / $\Delta\sigma$ is $2 \times 10^{-4}\,MPa^{-1}$, $3.3 \times 10^{-4}\,MPa^{-1}$, and $9.3 \times 10^{-4}\,MPa^{-1}$, respectively. These differences reflect the plastic deformation degree of the alloy to a certain extent, i.e., the deformation degree increases with increasing ratio. When the strain rate rises from 1000/s to 1500/s, the volume fraction of twins and martensite increases, and the value of $\Delta\varepsilon$ / $\Delta\sigma$ increases by $1.3 \times 10^{-4}\,MPa^{-1}$. Obviously, the increase of the plastic deformation degree of the alloy at this stage is closely related to the increase of the volume fraction of twins and martensite. When the strain rate rises up to 2000/s, adiabatic shear failure occurs, and the value of $\Delta\varepsilon$ / $\Delta\sigma$ increases sharply by $6 \times 10^{-4}\,MPa^{-1}$. The increase in the plastic deformation degree of the alloy at this stage is closely correlated with the occurrence of adiabatic shear failure.

Table 2
Unit strain increment induced by unit stress increment at different strain rates.

	$\dot{\varepsilon}_1$ = 1000/s	$\dot{\varepsilon}_2$ = 1500/s	$\dot{\varepsilon}_3$ = 2000/s
$\Delta\varepsilon/\Delta\sigma(10^{-4}\,MPa^{-1})$	2	3.3	9.3

Table 3
Average flow stress, true strain, and absorption energy of the alloy at different strain rates.

$\dot{\varepsilon}$	Average flow stress/MPa	True strain	Absorbed energy/(J/cm^3)
1000/s	928	0.055	45.4
1500/s	985	0.085	62.9
2000/s	1124	0.173	183.4

In addition, Mazeau [43] used the adiabatic shear localized energy as the basis for measuring the adiabatic shear sensitivity of different titanium alloys. The energy absorbed by the alloy during dynamic compression can be expressed as follows:

$$E = \int_0^{\varepsilon} \sigma \bullet \; d\varepsilon \tag{1}$$

In the above equation, σ and ε represent the true stress and the true strain, respectively. Table 3 shows the average flow stress, true strain, and absorbed energy of the alloy under dynamic compression at three strain rates. At strain rates of 1000/s, 1500/s, and 2000/s, the absorbed energy of the alloy is $45.4\,J/cm^3$, $62.9\,J/cm^3$, and $183.4\,J/cm^3$, respectively. Obviously, when the strain rate increases from 1000/s to 1500/s, the degree of plastic deformation is exacerbated due to the increase of the volume fraction of twins and martensite, which results in the alloy consuming more energy; when the strain rate rises up to 2000/s, the occurrence of adiabatic shear failure leads to further energy consumption.

3.3. The effect of twins and martensite on adiabatic shear behavior

A schematic of TEM observations illustrates that the size of the grain near the ASB is correlated with the distance from the ASB in the alloy. Fig. 7 shows a schematic of the area around the ASB and TEM images of a typical region subjected to a strain rate of 2000/s. As the figure shows, the alloy can be roughly divided into three areas: far away from the center of the ASB (denoted as **I**), close to the ASB (denoted as **II**), and inside the ASB (denoted as **III**). In area **I**, the twins and martensite are evenly distributed in the alloy. The TEM image in Fig. 7 shows a typical martensitic structure. In the image, the black region and the gray region correspond to the strain-induced martensite and the β phase, respectively. The phase boundary between the martensite and the matrix is relatively clear, and the dislocation density around the boundary is high, indicative of dislocation accumulation near this boundary. The underlying reason lies in the fact that the coordinated deformation between the two phases induces a large stress at the phase interface, leading to an increase in the dislocation density. In area **II**, i.e., close to the ASB, the plastic deformation becomes severe and dislocation accumulation in both phases is intensified, thus leading to the microstructure heavily deformed. In area **III**, the microstructure is mainly composed of the ultra-fine and equiaxed grains (size: ~200 nm). It is clearly seen that these small, equiaxed grains have well-defined boundaries. As reported [44,45], high shear stress leads to the lattice rotation of the deformed grains adjacent to the ASB, and the

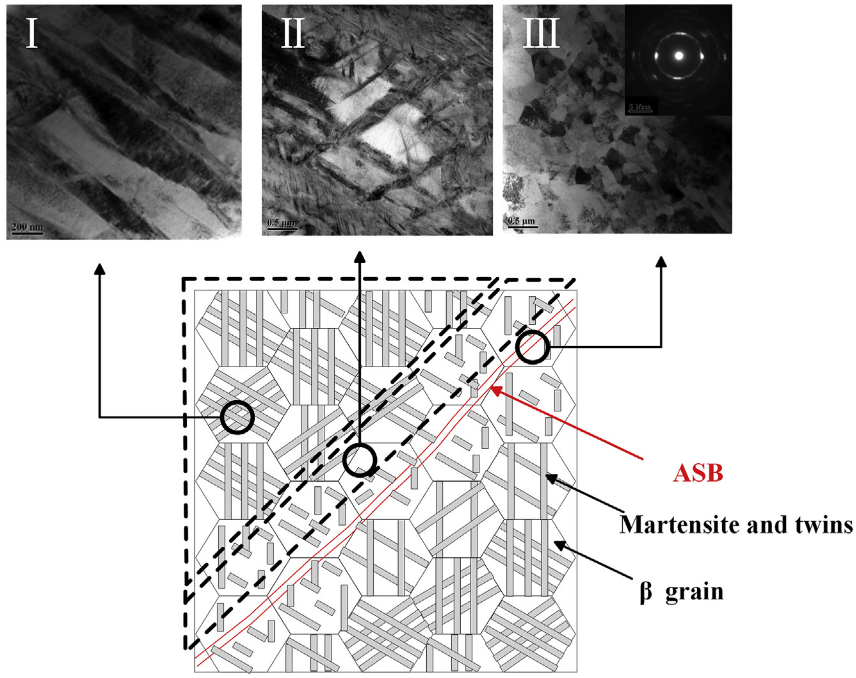

Fig. 7. Typical area near the ASB of the alloy and the corresponding schematic: (a) the area far away from the center of the ASB; (b) the area close to the ASB; (c) the area inside the ASB.

formation of the ultra-fine grains in the ASB should be attributed to the rotational dynamic recrystallization mechanism. Furthermore, Meyers et al. [46,47] demonstrated that the rotational dynamic recrystallization mechanism can reasonably explain the formation of ultra-fine grains in ASB by the thermodynamics and dynamics calculations. Moreover, the presence of DRXed grains is supported by the ring diffraction patterns inserted in area **III** of Fig. 7.

Based on the microstructural difference, ASBs are divided into deformed bands (DBs) and transformed bands (TBs) [48]. Generally, the DBs show the extensive plastic deformation characteristics, i.e. the severe deformed and elongated grains. The TBs are considered as the further development of the DBs. Therefore, more severe plastic deformation and higher temperature rising in the TBs than that of the DBs [49–52]. In the current study, the formed ASB at 2000/s is a typical transformed band, which is mainly composed of the ultra-fine and equiaxed grains, as shown in area III of Fig. 7.

TEM observations of the alloy at strain rate of 1000/s and 1500/s after dynamic compression are also conducted, as shown in Fig. 8(a) and (b). At strain rate of 1000/s (Fig. 8(a)), the boundary of martensite and the matrix, as well as dislocation accumulation near the boundary can be clearly seen. As strain rate increases to 1500/s (Fig. 8(b)), martensite has lost their original shape, and become fragmented due to severe deformation. As mentioned in Section 3.2, no ASB is observed at strain rate of 1000/s and 1500/s, and no dynamic recrystallization occurred.

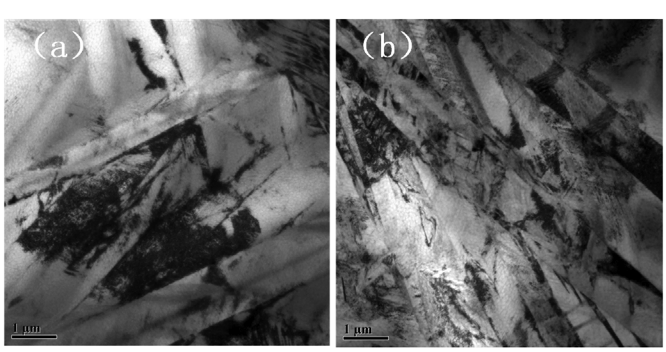

Fig. 8. TEM micrographs of the alloy at different strain rates: (a)1000/s; (b) 1500/s.

For additional microstructural analysis at the rate of 2000/s, we selected four regions referred to as ①, ②, ③, and ④ (see Fig. 5(c); the corresponding results are shown in Fig. 9 ①, ②, ③, and ④). Fig. 9 ① and ③ show SEM images of the areas adjacent to the ASBs in the alloy, while Fig. 9 ② and ④ show regions that are relatively far from the ASBs. Many twins and a large amount of martensite occur in the alloy, but the number of these structures is significantly lower near the ASBs. As can be seen from Fig. 5(a) and (b), the twins and martensite are originally distributed evenly in the alloy. During ASB initiation and formation, however, the twins and martensite in the vicinity of the ASBs are refined, owing to dislocation motion and dynamic recrystallization, which will absorb energy to some extent. Fig. 9① and ③ reveal the bifurcation of ASBs during the dynamic loading process. In fact, the local stress at these locations and the structural fluctuation increase, owing to the twins and martensite in the alloy, and ASB expansion is hindered by ASB interaction with these locations [53]. The expansion is also hindered by the twins and martensite perpendicular to the shear direction, as reported by Sun [18], resulting in a bifurcation of the ASBs. This distribution of the ASBs leads to dispersion of the plastic strain and plays a crucial role in the plasticity of the alloy [54–57].

4. Conclusions

In this study, the effect of twins and martensite on the adiabatic shear behavior in Ti-8.5Cr-1.5Sn alloy is systematically investigated and discussed. When the strain rate increases from 1000/s to 1500/s, the volume fraction of these features increases significantly, and the degree of plastic deformation is correspondingly intensified, thus resulting in an increase in the value of $\Delta\varepsilon \ / \ \Delta\sigma$. Adiabatic shear failure occurs when the strain rate reaches 2000/s. At this stage, the values of $\Delta\varepsilon/\Delta\sigma$ and the absorbed energy increase further, owing to the severe plastic deformation, DRX, and bifurcation of the ASBs. The TEM analysis shows that severe plastic deformation inside the ASBs leads to DRX, and the subsequent breaking of twins and martensite. Moreover, systematic SEM observation reveals that the presence of twins and

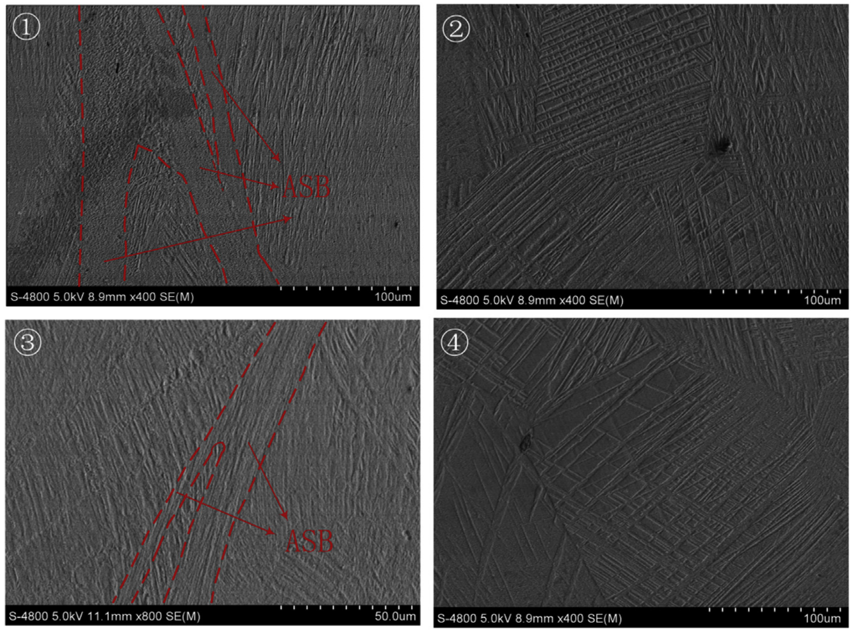

Fig. 9. SEM images showing four typical regions of the alloy at a strain rate of 2000/s: ① and ③ show the areas adjacent to the ASBs; ② and ④ show the regions far from the ASBs.

martensite induces (in general) bifurcation of the ASBs, which plays a crucial role in the plasticity of the alloy.

Data availability

The raw/processed data required to reproduce these findings cannot be shared at this time due to technical or time limitations.

Acknowledgments

This work was supported by the National Natural Science Foundation of China (Grant No. 51571031). Dr. You from University of Science & Technology Beijing is greatly appreciated for TEM tests.

References

[1] E.A.S. Jr, J.C. Williams, Progress in structural materials for aerospace systems1, Acta Mater. 51 (19) (2003) 5775–5799.
[2] O.M. Ivasishin, P.E. Markovsky, Y.V. Matviychuk, A comparative study of the mechanical properties of high-strength β-titanium alloys, J. Alloy. Comp. 457 (1–2) (2008) 0-309.
[3] F. Sun, F. Prima, T. Gloriant, High-strength nanostructured Ti–12Mo alloy from ductile metastable beta state precursor, Mater. Sci. Eng. A 527 (16) (2010) 4262–4269.
[4] Y.B. Xu, Y.L. Bai, M.A. Meyers, Deformation, phase transformation and recrystallization in the shear bands induced by high-strain rate loading in titanium and its alloys, J. Mater. Sci. Technol. 22 (6) (2006) 737–746.
[5] V.F. Nesterenko, M.A. Meyers, T.W. Wright, Self-organization in the initiation of adiabatic shear bands, Acta Mater. 46 (1) (1998) 327–340.
[6] Y.B. Xu, W.L. Zhong, Y.J. Chen, Shear localization and recrystallization in dynamic deformation of 8090 Al–Li alloy, Mater. Sci. Eng. A 299 (1–2) (2001) 287–295.
[7] Q. Xue, M.A. Meyers, V.F. Nesterenko, Self-organization of shear bands in titanium and Ti–6Al–4V alloy, Acta Mater. 50 (3) (2002) 575–596.
[8] V.F. Nesterenko, M.A. Meyers, T.W. Wright, Self-organization in the initiation of adiabatic shear bands, Acta Mater. 46 (1) (1998) 327–340.
[9] B. Dobb, Y.L. Bai, Adiabatic Shear Localization: Frontiers and Advances, (2012) Amsterdam.
[10] L. Kuang, Z. Chen, Y. Jiang, Adiabatic shear behaviors in rolled and annealed pure titanium subjected to dynamic impact loading, Mater. Sci. Eng. A 685 (2017) 95–106.
[11] Y. Jiang, Z. Chen, C. Zhan, Adiabatic shear localization in pure titanium deformed by dynamic loading: microstructure and microtexture characteristic, Mater. Sci. Eng. A 640 (2015) 436–442.
[12] J. Peirs, W. Tirry, B. Amin-Ahmadi, Microstructure of adiabatic shear bands in Ti6Al4V, Mater. Char. 75 (2) (2013) 79–92.
[13] X. Xu, L. Wang, D.H. Zhao, Dynamic behavior in Ti-5553 alloy with β phase under compression loading, Appl. Mech. Mater. 782 (2015) 88–96.
[14] G. Sukumar, B.B. Singh, A. Bhattacharjee, Ballistic impact behaviour of β-CEZ Ti alloy against 7.62mm armour piercing projectiles, Int. J. Impact Eng. 54 (1) (2013) 149–160.
[15] X.H. Min, X.J. Chen, S. Emura, K. Tsuzaki, Quantitative Analysis of Twinning-Induced Plasticity (TWIP) in Beta-Titanium Alloy, John Wiley and Sons, Inc, 2013.
[16] F. Sun, J.Y. Zhang, P. Vermaut, D. Choudhuri, T. Alam, S.A. Mantri, P. Svec, T. Gloriant, P.J. Jacques, Strengthening strategy for a ductile metastable β-titanium alloy using low-temperature aging, Proceedings of the 13th World Conference on Titanium, John Wiley and Sons, Inc, 2016.
[17] S. Osovski, D. Rittel, P. Landau, Microstructural effects on adiabatic shear band formation, Scripta Mater. 66 (1) (2012) 9–12.
[18] X.R. Sun, H.Z. Wang, P. Yang, Mechanical behaviors and micro-shear structures of metals with different structures by high-speed compression, Acta Metall. Sin. 50 (4) (2014) 387–394.
[19] V.F. Zackay, E.R. Parker, D. Fahr, R.A. Busch, The enhancement of ductility in high-strength steels, ASM Trans. Quart. 60 (2) (1967) 252–259.
[20] C. Brozek, F. Sun, P. Vermaut, Y. Millet, Development of new trip/twip titanium alloys combining high strength, high strain hardening and improved ductility, Proceedings of the 13th World Conference on Titanium, 2016.
[21] J. Yan, TRIP Titanium Alloy Design, Northwestern University, 2014.
[22] M. Eskandari, M.A. Mohtadi-Bonab, A. Zarei-Hanzaki, A.G. Odeshi, J.A. Szpunar, High-resolution EBSD study of adiabatic shear band and neighboring grains after dynamic impact loading of Mn-steel used in vehicle structure, J. Mater. Eng. Perform. 25 (4) (2016) 1611–1620.
[23] C. Brozek, F. Sun, P. Vermaut, A β-titanium alloy with extra high strain-hardening rate: design and mechanical properties, Scripta Mater. 114 (2016) 60–64.
[24] D. Kuroda, M. Niinomi, M. Morinaga, Design and mechanical properties of new β-type titanium alloys for implant materials, Mater. Sci. Eng. A 243 (1–2) (1998) 244–249.
[25] M. Abdel-Hady, K. Hinoshita, M. Morinaga, General approach to phase stability and elastic properties of β-type Ti-alloys using electronic parameters, Scripta Mater. 55 (5) (2006) 477–480.
[26] S.G. Steinemann, P.A. Mäusli, Titanium Alloys for Surgical Implants-Biocompatibility from Physicochemical Principles, Sixth World Conference on Titanium, Cannes, 1988.
[27] K.S. Vecchio, F. Jiang, Improved pulse shaping to achieve constant strain rate and stress equilibrium in split-hopkinson pressure bar testing, Metall. Mater. Trans. A 38 (11) (2007) 2655–2665.
[28] D.J. Frew, M.J. Forrestal, W. Chen, Pulse shaping techniques for testing brittle materials with a split hopkinson pressure bar, Exp. Mech. 42 (1) (2002) 93–106.
[29] E.O. Hall, The deformation and ageing of mild steel : II characteristics of the luders deformation, Proc. Phys. Soc. 64 (9) (1951) 742.
[30] N.J. Petch, J. Iron Steel Inst, London 174 (1953) 25.
[31] M.R. Barnett, A rationale for the strong dependence of mechanical twining on grain size, Scripta Mater. 59 (14) (2008) 696–698.
[32] B. Gumus, B. Bai, G. Gersteing, Twinning activities in high-Mn austenitic steels under highvelocity compressive loading, Mater. Sci. Eng. A 648 (11) (2015) 104–112.
[33] J.C. Russ, R.T. Dehoff, Practical Stereology, second ed., (1999) New York.
[34] J.W. Christian, S. Mahajan, Prog. Mater. Sci. 39 (1995) 1–157.

[35] B.B. Ai, Study on Annealing Microstructure and Mechanical Properties of TRIP/TWIP Steel Plate by Cold Rolling and High Rolling, (2013) Changsha.
[36] F. Zhen, K. Zhang, Z.L. Guo, Effect of martensite fine structure on mechanical properties of an 1100 MPa grade ultra-high strength steel, J. Iron Steel Res. Int. 22 (7) (2015) 645–651.
[37] X.H. Yuan, M.S. Yang, K.Y. Zhao, Effects of microstructure transformation on strengthening and toughening for heat-treated low carbon martensite stainless bearing steel, Mater. Sci. Forum 817 (2015) 667–674.
[38] G. Saul, J.A. Roberson, A.M. Adair, The effects of thermal treatment on the austenitic grain size and mechanical properties of 18 Pct Ni maraging steels, Metall. Mater. Trans. B 1 (2) (1970) 383–387.
[39] A.Q. Khan, G. Perre, L. Delaey, Stress-induced phase transformations and enhanced plasticity in copper-aluminium and copper-aluminium-zinc martensites, J. Mater. Sci. 7 (12) (1972) 1401–1408.
[40] E.S. Puchi-Cabrera, M.H. Staia, J.D. Guérin, An experimental analysis and modeling of the work-softening transient due to dynamic recrystallization, Int. J. Plast. 54 (2014) 113–131.
[41] P. Landau, S. Osovski, A. Venkert, The genesis of adiabatic shear bands, Sci. Rep. 6 (2016) 37226.
[42] A. Grajcar, R. Kuziak, Dynamic recrystallization behavior and softening kinetics in 3Mn-1.5Al TRIP steels, Adv. Mater. Res. 287–290 (2011) 330–333.
[43] C. Mazeau, L. Beylat, P. Longère, P. Louvigné, On the quantitative evaluation of adiabatic shear banding sensitivity of various titanium alloys, J. Phys. IV (1997) France.
[44] M.A. Meyers, G. Subhash, B.K. Kad, Evolution of microstructure and shear-band formation in α-hcp titanium, Mech. Mater. 17 (2–3) (1994) 175–193.
[45] M.A. Meyers, V.F. Nesterenko, J.C. Lasalvia, Shear localization in dynamic deformation of materials: microstructural evolution and self-organization, Mater. Sci. Eng. A 317 (1–2) (2001) 204–225.
[46] M.A. Meyers, Y.B. Xu, Q. Xu, Microstructural evolution in adiabatic shear localization in stainless steel, Acta Mater. 51 (5) (2003) 1307–1325.
[47] M.A. Meyers, V.F. Nesterenko, J.C. Lasalvia, Shear localization in dynamic deformation of materials: microstructural evolution and self-organization, Mater. Sci. Eng. A 317 (1) (2001) 204–225.
[48] G.A. Li, L. Zhen, C. Lin, Deformation localization and recrystallization in TC4 alloy under impact condition, Mater. Sci. Eng. A 395 (1–2) (2005) 98–101.
[49] Q. Xue, G.T. Gray, Development of adiabatic shear bands in annealed 316L stainless steel: Part II. TEM studies of the evolution of microstructure during deformation localization, Metall. Mater. Trans. A 37 (8) (2006) 2447–2458.
[50] M.A. Meyers, Y.B. Xu, Q. Xue, Microstructural evolution in adiabatic shear localization in stainless steel, Acta Mater. 51 (5) (2003) 1307–1325.
[51] M.T. Pérez-Prado, J.A. Hines, K.S. Vecchio, Microstructural evolution in adiabatic shear bands in Ta and Ta-W alloys, Acta Mater. 49 (15) (2001) 2905–2917.
[52] D.R. Chichili, K.T. Ramesh, K.J. Hemker, Adiabatic shear localization in α-titanium: experiments, modeling and microstructural evolution, J. Mech. Phys. Solids 52 (8) (2004) 1889–1909.
[53] Y.J. Sun, D.W. Xing, Y.J. Huang, J. Shen, A new type of Zr-Al-Ni-Cu bulk metallic glass with high plasticity at room temperature, Rare Metal Mater. Eng. 38 (38) (2009) 54–58.
[54] E.S. Park, J.S. Kyeong, D.H. Kim, Phase separation and improved plasticity by modulated heterogeneity in Cu–(Zr, Hf)–(Gd, Y)–Al metallic glasses, Scripta Mater. 57 (1) (2007) 49–52.
[55] U. Kühn, N. Mattern, A. Gebert, Nanostructured Zr- and Ti-based composite materials with high strength and enhanced plasticity, J. Appl. Phys. 98 (5) (2005) 171–243.
[56] C. Fan, D. Qiao, T.W. Wilson, As-cast Zr–Ni–Cu–Al–Nb bulk metallic glasses containing nanocrystalline particles with ductility, Mater. Sci. Eng. A 431 (1) (2006) 158–165.
[57] K. Mondal, T. Ohkubo, T. Toyama, The effect of nanocrystallization and free volume on the room temperature plasticity of Zr-based bulk metallic glasses, Acta Mater. 56 (18) (2008) 5329–5339.